

Added damping of a wind turbine rotor: Two-dimensional discretization expressing the nonlinear wind-force dependency

P. van der Male¹, K.N. van Dalen², A.V. Metrikine²

¹Department of Hydraulic Eng., Faculty of Civil Engineering and Geosciences, Delft University of Technology, Stevinweg 1 2628 CN Delft, the Netherlands

²Department of Structural Eng., Faculty of Civil Engineering and Geosciences, Delft University of Technology, Stevinweg 1 2628 CN Delft, the Netherlands

email: p.vandermale@tudelft.nl, k.n.vandalen@tudelft.nl, a.metrikine@tudelft.nl

ABSTRACT: In determining wind forces on wind turbine blades, and subsequently on the tower and the foundation, the blade response velocity cannot be neglected. This velocity alters the wind force, which depends on the wind velocity relative to that of the blades. This blade response velocity component of the wind force is commonly referred to as added damping. The relation between the relative wind velocity and the actual wind forcing is nonlinear. Moreover, the wind excitation couples the flap and edge wise blade motion. This work analyzes both the nonlinear excitation and the coupling of the lateral blade motions. To this end, a single blade is modelled as a cantilever beam, which is exposed to the nonlinear wind excitation. Flap and edge wise blade motions are coupled via the wind forcing. Thereupon, the continuous model, described by a system of partial differential equations, is reduced to a two-degree-of-freedom system, accounting for the principal flap and edge wise modes only. The dynamic response is determined in the frequency domain for a blade of the academic NREL5 turbine. The response to the quadratic terms in the force formulation is determined with the help of the Volterra series expansion, in combination with the harmonic balance technique. Results are presented for a blade of both a non-operating and an operating turbine, where a band-limited white noise input signal was applied. The quadratic terms in the forcing equations do not contribute much to the total responses. For some second order responses, however, negative added damping due to the structural motion is observed.

KEY WORDS: Aerofoils, quadratic excitation, added damping, modal decomposition, Volterra series expansion.

1 INTRODUCTION

The rotor of a wind turbine acts as a damper for the dynamic response of its tower and foundation structure. Not only does this apply directly for the response to aerodynamic forcing, the response to the hydrodynamic forcing of offshore wind turbines is damped by the rotor too. The damping effect results from the motion of the rotor blades relative to the ambient wind velocity. This damping is commonly referred to as aerodynamic damping.

In order to improve understanding of the damping effect of a rotor as a whole, the wind-structure interaction of a single blade needs to be fully understood. First of all, wind excitation couples flap and edge wise blade motion. Second, the actual forcing depends nonlinearly on the relative wind velocity. For wind turbine blades an additional nonlinearity is introduced by the aeroelastic coefficients, which represent the shape of the blade and the nature of the response as a function of the wind angle of attack.

Previous research has predominantly been devoted to the effect of the nonlinear aeroelastic coefficients. The work done by Hansen et al. [1] can be mentioned as representative example, in which a nonlinear aeroelastic model is described, explicitly accounting for a time-varying angle of attack and separation of airflow. An alternative approach was presented by Riziotis et al. [2], where linear inviscid and nonlinear viscous force contributions are distinguished. A similar aeroelastic model was adopted before by Chaviaropoulos [3], who addressed the combined flap and edge wise response of turbine blades.

The existing studies have in common that the wind velocity dependence of the wind forcing has been linearized. This simplification neglects both second order forcing and associated added damping components. Analysis of the contribution of these nonlinear terms is a specific purpose of this work. A single blade is modelled as a cantilever beam, which is exposed to the nonlinear wind excitation. Flap and edge wise blade motion are coupled via a force formulation. Thereupon, the continuous model, described by a system of partial differential equations, is reduced to a two-degree-of-freedom (2DOF) model, accounting for the principal flap and edge wise modes only.

Systems containing nonlinearities of the polynomial type can be analyzed in the frequency domain with the application of the Volterra series expansion [4]. With this technique, higher order system characteristics are expressed by higher order Volterra kernels. For fairly simple systems, these kernels can be identified with the help of the harmonic balance technique [5]. Worden et al. [6] described the kernel identification for multi-input multi-output systems. The application of the Volterra series expansion to nonlinear fluid-structure interaction problems cannot be called novel. Wind-excited structures have been addressed by a number of researchers [7-10]. Systems sensitive for added damping have been studied by Kareem et al. [11], and more recently by Carassale and Kareem [12]. Balajewicz [13] applied the Volterra expansion to a two degree of freedom airfoil undergoing simultaneously forced pitch and heave.

To determine the dynamic response of an actual turbine, the blade characteristics of the NREL5 turbine are adopted [14].

Responses for a non-operating feathered blade and a rotating blade are determined, on which basis both the contribution of the second order forcing and the total added damping are identified. In achieving the latter, a comparison with a system without added damping has been made.

2 MODEL DESCRIPTION

2.1 Blade model

A turbine blade is modelled as a cantilever beam of length R , rigidly fixed to the hub (see Figure 1). The beam is described within a rotating frame of reference. The r axis represents the longitudinal axis of the undeformed blade, where the origin coincides with the point of rotation.

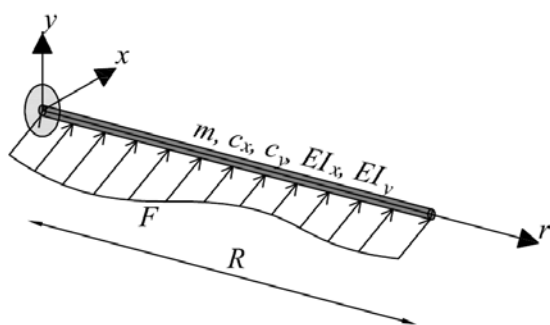


Figure 1. Blade model.

Figure 2 presents a cross section of the blade, in which the x and y axes coincide with its principal axes; the x axis represents the weak and the y axis the strong axis. The XY coordinate system is adopted to describe flap and edge wise blade motion; the X axis coincides with the plane of rotation and the Y axis is directed normal to this plane. The angle β describes the angle between the local x and the global X axis, and is composed of both fixed blade twist and varying blade pitch. The blade twist generally varies along the longitudinal axis. Here, the blade twist is taken constant.

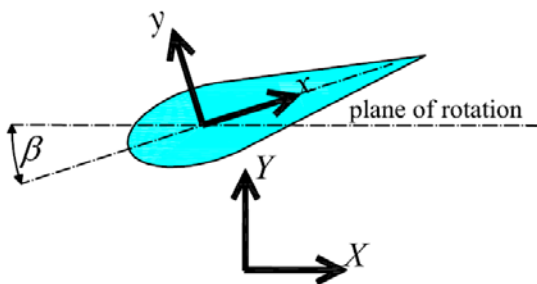


Figure 2. Blade cross-section.

In accordance with Burton et al. [15], the blade is described as a geometrically linear Euler-Bernoulli beam. The initially uncoupled equations of motion for deformation in x and y direction – combined in the vector \mathbf{u} – read:

$$\mathbf{m} \frac{\partial^2 \mathbf{u}}{\partial t^2} + \mathbf{c} \frac{\partial \mathbf{u}}{\partial t} + \left(\frac{\partial^2}{\partial r^2} \left(\mathbf{EI} \frac{\partial^2}{\partial r^2} \right) - \frac{\partial}{\partial r} \left(\mathbf{T} \frac{\partial}{\partial r} \right) \right) \mathbf{u} = \mathbf{F}. \quad (1)$$

Both the displacement vector \mathbf{u} and the force vector \mathbf{F} comprise an x and a y component. The coefficient matrices are

all diagonal; \mathbf{m} describes the distributed mass, \mathbf{c} represents the structural damping, which is assumed to be proportional to mass and stiffness, \mathbf{EI} consists of the bending stiffness components with respect to the principal axes, which vary with r , and \mathbf{T} describes the tension, resulting from rotation of the blade.

2.2 Force definition: drag and lift

Figure 3(a) depicts a cross section of the blade model, subjected to an air flow \mathbf{W} . The local width of the aerofoil is given by c and α represents the angle between the flow vector and the local x axis, the so-called angle of attack.

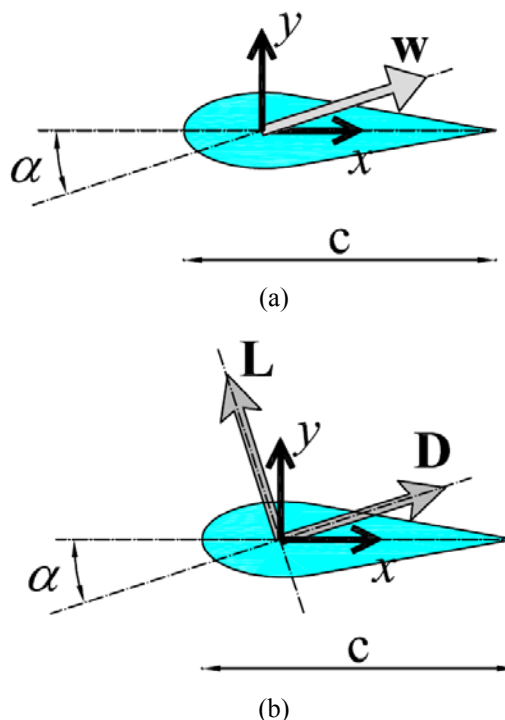


Figure 3. (a) Blade cross-section exposed to a wind velocity vector \mathbf{W} with an angle of attack α . (b) Lift and drag force definitions, resulting from the vector \mathbf{W} .

An aerofoil situated in an air flow experiences a force parallel to the direction of the flow and a force perpendicular to the flow direction – drag and lift respectively – as presented in Figure 3(b). In this paper, drag is restricted to viscous drag, and can be expressed as:

$$\mathbf{D} = \frac{1}{2} \rho c C_d \mathbf{W} |\mathbf{W}|, \quad (2)$$

where ρ the air density and C_d is the Reynolds number dependent drag coefficient, accounting for the frictional stresses that can develop as a result of the air flow. The lift force for attached flow can be determined from [15]:

$$\mathbf{L} = \rho (\mathbf{\Gamma} \times \mathbf{W}) \quad (3)$$

where $\mathbf{\Gamma}$ is the air circulation strength, defined as:

$$\Gamma = \frac{1}{2} C_l c |\mathbf{W}| \mathbf{e}_r. \quad (4)$$

\mathbf{e}_r is the unit vector along the local r axis. The lift coefficient C_l can for relatively small angles α be expressed as:

$$C_l = 2\pi \sin \alpha. \quad (5)$$

The force vector \mathbf{F} is a function of r and time t . Of its constituents, the air flow vector \mathbf{W} is both r and t dependent, as is automatically the angle of attack α . The chord width c and the drag coefficient C_d vary in space only, if the Reynolds number dependency of the latter is neglected

2.3 Constituents of the air flow vector

Both drag and lift are defined in relation to the air flow vector \mathbf{W} , which is positioned with an angle α to the local x axis of the aerofoil. Figure 4 presents the vector \mathbf{W} , which is active under the angle α with respect to the symmetry axis of the aerofoil and the angle φ with respect to the plane of rotation. The vector \mathbf{W} can be thought of as a summation of vectors:

$$\mathbf{W} = \bar{\mathbf{W}} + \mathbf{w} - \frac{\partial \mathbf{u}}{\partial t}, \quad (6)$$

where $\bar{\mathbf{W}}$ represents the mean air flow velocity and \mathbf{w} the velocity fluctuations around the mean. The time derivative of \mathbf{u} represents the structural response velocity, which is responsible for the added damping.

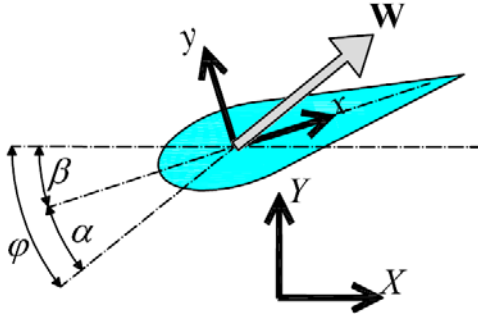


Figure 4. Pitched blade cross-section exposed to a wind velocity vector \mathbf{W} with an angle of attack α .

Physical understanding of these components can be obtained when considering these vector terms within the global frame of reference. The Y component of $\bar{\mathbf{W}}$ represents the mean wind velocity perpendicular to the rotational plane. Within the plane of rotation, the mean air flow velocity equals the tangential velocity of the aerofoil, calculated from the rotational speed of the rotor Ω and the r coordinate of the aerofoil cross section under consideration.

The air flow fluctuations of the \mathbf{w} vector are related to ambient aerodynamics, such as the turbulence intensity and the turbulence length scale. Both out-of-plane and in-plane wind fluctuations w_x and w_y , respectively, can be determined on the basis of existing wind turbulence spectra. In both cases, the wind fluctuation needs to be corrected for the rotation of the aerofoil. In addition to this, the aerofoil experiences the

mean in-plane wind velocity \bar{W}_x as a sinusoidal varying air flow.

In order to incorporate these vectors in the equations of motion, the vector components need to be transformed to the local reference system by rotation over the angle β . After transformation to the local reference system, the vector components are referred to as W_x and W_y , and follow from:

$$\bar{\mathbf{W}} = \begin{bmatrix} \bar{W}_x \\ \bar{W}_y \end{bmatrix} = \begin{bmatrix} (\Omega r \cos \beta + \bar{W}_y \sin \beta) \\ (\bar{W}_y \cos \beta - \Omega r \sin \beta) \end{bmatrix}, \text{ and} \quad (7)$$

$$\mathbf{w} = \begin{bmatrix} w_x \\ w_y \end{bmatrix} = \begin{bmatrix} ((w_x + \bar{W}_x \cos(\Omega t)) \cos \beta + w_y \sin \beta) \\ (w_y \cos \beta - (w_x + \bar{W}_x \cos(\Omega t)) \sin \beta) \end{bmatrix} \quad (8)$$

2.4 Modal decomposition

The motion of the turbine blade is described by a system of coupled nonlinear partial differential equations, allowing for motions in both x and y direction, see Equation (1). Coupling takes place via the forcing term, due to the structural response velocity. Likewise, the nonlinearity is pronounced in the forcing term, since eventually in both drag and lift forcing terms the multiplication $\mathbf{W}|\mathbf{W}|$ appears.

Due to the presence of the damping and the centrifugal stiffening term, the system of differential equations contains operators that are not self-adjoint, implying that no classical, i.e., real, dynamic modes with fixed nodes exist. In order to identify structural modes of vibration, a phase shift within each mode should be accounted for.

Despite the nonlinear components and the presence of non-classical damping, the system of partial differential equations is reduced to a system of ordinary differential equations by means of modal decomposition. Both x and y are expressed as an infinite series of generalized coordinates q and shape functions ψ :

$$u_x = \sum_{n=1}^{\infty} q_x^{(n)} \psi_x^{(n)}, \text{ and} \quad (9)$$

$$u_y = \sum_{n=1}^{\infty} q_y^{(n)} \psi_y^{(n)} \quad (10)$$

The adopted shapes functions, or modes, correspond to those of an undamped and untensioned blade. Since these modes do not fulfil the orthogonality conditions with respect to all differential operators, the initial partial differential equations cannot be decomposed into a system of uncoupled ordinary differential equations. By restricting the decomposition to the first modes for both x and y directions, a system of two ordinary differential equations can be obtained, only coupled via the structural response velocity. After multiplication of both differential equations by $\psi_x^{(1)}$ and $\psi_y^{(1)}$, respectively, and integration over r , the following ordinary differential equations remain:

$$M_x \frac{d^2 q_x^{(1)}}{dt^2} + C_x \frac{dq_x^{(1)}}{dt} + K_x q_x^{(1)} = \int_0^R F_x^{(1)} \psi_x^{(1)} dr, \text{ and} \quad (11)$$

$$M_y \frac{d^2 q_y^{(1)}}{dt^2} + C_y \frac{dq_y^{(1)}}{dt} + K_y q_y^{(1)} = \int_0^R F_y^{(1)} \psi_y^{(1)} dr \quad (12)$$

The corresponding 2DOF system is illustrated by Figure 5.

2.5 Force decomposition

In order to take a closer look at the right hand sides of the sets of differential equations, first the scalar equations of the forcing vector \mathbf{F} are presented:

$$F_x = D_x + L_x = \frac{1}{2} \rho c C_d |\mathbf{W}| W_x - \frac{1}{2} \rho c C_l |\mathbf{W}| W_y \quad (13)$$

$$F_y = D_y + L_y = \frac{1}{2} \rho c C_d |\mathbf{W}| W_y + \frac{1}{2} \rho c C_l |\mathbf{W}| W_x \quad (14)$$

It can immediately be recognized that the decomposition concerns the multiplications $|\mathbf{W}| W_x$ and $|\mathbf{W}| W_y$.

Furthermore, the aeroelastic coefficients C_d and C_l are α dependent. Equation (5) introduced a simple relation between C_l and α , which is valid for attached flows. With reference to Figure 4, the following expression can be derived:

$$\sin \alpha = \frac{W_y}{|\mathbf{W}|} \quad (15)$$

This expression reveals the time dependency of the angle of attack and introduces an additional coupling between the motions in x and y direction. It should be noted that blade torsion, mainly resulting from the twisted shape of the blade, brings an important contribution to the time variation of the angle of attack α . Since the twist angle is neglected in the current analysis, no α variation due to torsion takes place.

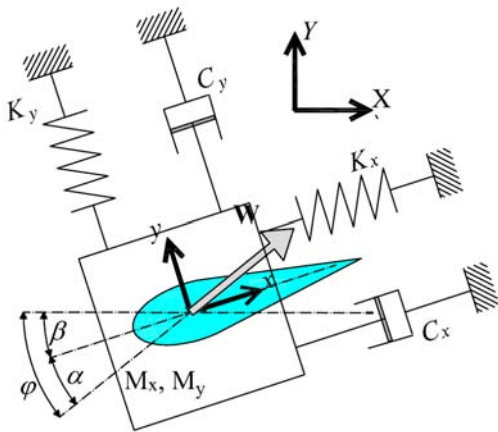


Figure 5. 2DOF representation of the turbine blade.

The drag coefficient C_d is assumed to be α independent. This assumption is valid for relatively small values of α . This condition was already adopted for the lift coefficient C_l . Applying now the modal decomposition gives the following expressions for F_x and F_y :

$$F_x^{(1)} = \frac{1}{2} \rho c C_d \left(\bar{W}_x + w_x - \frac{dq_x^{(1)}}{dt} \psi_x^{(1)} \right) \times \sqrt{\left(\bar{W}_x + w_x - \frac{dq_x^{(1)}}{dt} \psi_x^{(1)} \right)^2 + \left(\bar{W}_y + w_y - \frac{dq_y^{(1)}}{dt} \psi_y^{(1)} \right)^2} \quad (16)$$

$$- \pi \rho c \left(\bar{W}_y + w_y - \frac{dq_y^{(1)}}{dt} \psi_y^{(1)} \right)^2$$

$$F_y^{(1)} = \frac{1}{2} \rho c C_d \left(\bar{W}_y + w_y - \frac{dq_y^{(1)}}{dt} \psi_y^{(1)} \right) \times \sqrt{\left(\bar{W}_x + w_x - \frac{dq_x^{(1)}}{dt} \psi_x^{(1)} \right)^2 + \left(\bar{W}_y + w_y - \frac{dq_y^{(1)}}{dt} \psi_y^{(1)} \right)^2} \quad (17)$$

$$+ \pi \rho c \left(\bar{W}_x + w_x - \frac{dq_x^{(1)}}{dt} \psi_x^{(1)} \right) \left(\bar{W}_y + w_y - \frac{dq_y^{(1)}}{dt} \psi_y^{(1)} \right)$$

In accordance with Equation (11) and (12) both expressions need to be multiplied with ψ_x^1 and ψ_y^1 , respectively, and integrated with respect to r over the interval $0 \leq r \leq R$. It should be noted that in general the chord width c and the drag coefficient C_d are r dependent. The same applies for the tangential velocity of the aerofoil \bar{W}_x , which is calculated from the rotational speed of the rotor Ω and r .

3 VOLTERRA SERIES EXPANSION

Nonlinearities of the polynomial type can be dealt with in the frequency domain by means of the Volterra series expansion. With the application of this method, the frequency dependent structural responses $Q_x^{(1)}$ and $Q_y^{(1)}$ can be written as an infinite series:

$$Q_j^{(1)} = \sum_{i=1}^{\infty} Q_j^{(1;i)}, \text{ for } j = x, y. \quad (18)$$

The superscript (1) refers to the modal shape, which was adopted to derive the generalized coordinates. From here on, this superscript will be omitted. Each component $Q_j^{(i)}$ can be expressed in terms of the input functions \tilde{W}_x and \tilde{W}_y – where the tilde indicates the frequency domain representation of w_x and w_y – and the Volterra kernels $H_j^{(i)}$. From the first order Volterra kernels, linear transfer functions can be recognized instantly. In the specific case of the system under consideration, the first order term of the Volterra series yields

$$Q_j^{(1)}(\omega) = H_{j;x}^{(1)}(\omega) \tilde{W}_x(\omega) + H_{j;y}^{(1)}(\omega) \tilde{W}_y(\omega). \quad (19)$$

The explicit reference to the frequency dependency is adopted for convenience sake. For the second order term it follows:

$$\begin{aligned}
 Q_j^{(2)}(\omega) &= \frac{1}{2\pi} \int_{-\infty}^{\infty} H_{j;xx}^{(2)}(\omega_1, \omega - \omega_1) \tilde{W}_x(\omega_1) \tilde{W}_x(\omega - \omega_1) d\omega_1 \\
 &+ \frac{1}{2\pi} \int_{-\infty}^{\infty} H_{j;yy}^{(2)}(\omega_1, \omega - \omega_1) \tilde{W}_y(\omega_1) \tilde{W}_y(\omega - \omega_1) d\omega_1 \quad (20) \\
 &+ \frac{1}{2\pi} \int_{-\infty}^{\infty} H_{j;xy}^{(2)}(\omega_1, \omega - \omega_1) \tilde{W}_x(\omega_1) \tilde{W}_y(\omega - \omega_1) d\omega_1
 \end{aligned}$$

, where both the Volterra kernels and the input signals are a function of ω and ω_1 .

An elegant method to derive the Volterra kernels is the harmonic probing technique, which is based on the idea that a harmonic input results in a harmonic output. For instance, by stating that

$$w_x = e^{i\omega t}, w_y = 0, \text{ and} \quad (21)$$

$$q_x^{(1)} = H_{x;x}^{(1)}(\omega) e^{i\omega t}, q_y^{(1)} = H_{y;x}^{(1)}(\omega) e^{i\omega t}, \quad (22)$$

the first order Volterra kernels can be obtained by solving the algebraic equations for the coefficients of $e^{i\omega t}$ only. The same procedure applies for the second order kernels, where the input and output take the form

$$w_x = e^{i\omega_1 t} + e^{i\omega_2 t}, w_y = 0, \text{ and} \quad (23)$$

$$\begin{aligned}
 q_x^{(2)} &= H_{x;x}^{(1)}(\omega_1) e^{i\omega_1 t} + H_{x;x}^{(1)}(\omega_2) e^{i\omega_2 t} \\
 &+ 2H_{x;xx}^{(2)}(\omega_1, \omega_2) e^{i(\omega_1 + \omega_2)t} \quad (24)
 \end{aligned}$$

$$\begin{aligned}
 q_y^{(2)} &= H_{y;x}^{(1)}(\omega_1) e^{i\omega_1 t} + H_{y;x}^{(1)}(\omega_2) e^{i\omega_2 t} \\
 &+ 2H_{y;xx}^{(2)}(\omega_1, \omega_2) e^{i(\omega_1 + \omega_2)t} \quad (25)
 \end{aligned}$$

The second order kernels can be derived from the terms containing $e^{i(\omega_1 + \omega_2)t}$. For the input frequencies it should apply that $\omega_1 + \omega_2 = \omega$. The procedure must be repeated for zero w_x and double harmonic w_y input, to derive the $H_{x;yy}^{(2)}(\omega_1, \omega_2)$ and $H_{y;yy}^{(2)}(\omega_1, \omega_2)$ kernels. The cross-kernels follow from

$$w_x = e^{i\omega_1 t}, w_y = e^{i\omega_2 t} \quad (26)$$

$$\begin{aligned}
 q_x^{(2)} &= H_{x;x}^{(1)}(\omega_1) e^{i\omega_1 t} + H_{x;y}^{(1)}(\omega_2) e^{i\omega_2 t} \\
 &+ 2H_{x;xy}^{(2)}(\omega_1, \omega_2) e^{i(\omega_1 + \omega_2)t} \quad (27)
 \end{aligned}$$

$$\begin{aligned}
 q_y^{(2)} &= H_{y;x}^{(1)}(\omega_1) e^{i\omega_1 t} + H_{y;y}^{(1)}(\omega_2) e^{i\omega_2 t} \\
 &+ 2H_{y;xy}^{(2)}(\omega_1, \omega_2) e^{i(\omega_1 + \omega_2)t} \quad (28)
 \end{aligned}$$

The response to finite order polynomials can be determined exactly with the application of the Volterra series expansion in combination with the harmonic probing technique. polynomials of infinite order, however, require truncation in order to suit Volterra analysis. The same applies for finite order polynomials that consist of too many terms, since for higher order kernels the method becomes computationally expensive.

To facilitate the harmonic balance technique, a Taylor series expansion is applied to the right hand sides of the equations of

motion, Equation (16) and (17). The input and output variables w_x , w_y , q_x and q_y are taken as expansion variables. Expansion is carried out to the third order, implying that linear and quadratic components are accounted for.

4 CASE STUDY

4.1 NREL5 turbine

To analyze the structural response of a wind turbine blade, the blade characteristics of the academic NREL5 turbine are adopted [14]. A typical aspect of these blades is the relatively high Lock number, which expresses the aerodynamic lift capability of a blade in comparison to its weight. As a result of this, other researchers – among which Bir and Jonkman (2007) [16] – have found high aerodynamic damping values, which may be not in the same range as for other turbine types. The first flap wise natural frequency, for bending around the local x axis, is approximately 4.21 rad/s; whereas the first edge wise natural frequency is approximately 6.79 rad/s.

4.2 Excitation

The dynamic responses are determined on the basis of a relatively simple input signal, which can be described as:

$$\tilde{W} = \tilde{W}_x = \tilde{W}_y, \text{ and} \quad (29)$$

$$\tilde{W} = |\tilde{W}| e^{i\theta}. \quad (30)$$

This signal is applied simultaneously in x and y direction. The amplitude is given a value larger than zero, only within the frequency intervals from -5.0 rad/s to -0.5 rad/s and from +0.5 rad/s to +5.0 rad/s. θ represents a random phase angle as a function of the excitation frequency ω , with values in the range from $-\pi$ to $+\pi$. In the time domain, the excitation function represents a noisy signal, consisting of frequencies from +0.5 rad/s to +5.0 rad/s. The input content at negative frequencies is taken into account to correctly carry out the convolution of Equation (20). The signal is defined with frequency steps of 0.1 rad/s.

4.3 Non-operating turbine

First, the response of a standstill blade is analyzed. The blade is assumed to be pointing upwards and feathered into the direction of the mean wind velocity. A feathered blade is pitched over an angle $\frac{1}{2}\pi$, implying that both drag and lift are as small as possible. The mean wind velocity is 10 m/s. The amplitude of the excitation signal is chosen such that the maximum amplitude in the time domain is approximately 1.0 m/s. This corresponds to an uniform amplitude $|\tilde{W}|$ of the band-limited white noise signal of 0.4 m. The aeroelastic drag coefficient is set at 0.1, irrespective of the angle of attack. The lift coefficient follows from Eq. (5).

Figure 6 presents the linear frequency-domain responses. Only the results for positive frequencies are presented. As could have been expected, the motion only takes place within the frequency interval of the excitation signal. In absence of a mean wind component normal to the feathered blade, only a cross-flow response in y direction takes place.

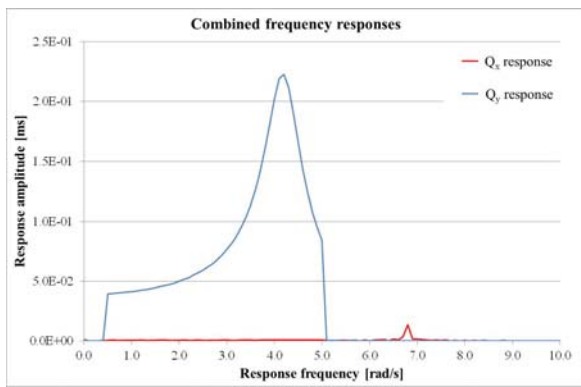


Figure 6. First order frequency responses non-operating turbine blade.

The second order responses, which are presented in Figure 7, mainly show content for the $Q_{x,xx}^2$ response. The peak response is observed at the first natural frequency for motion in x direction. The input signal does not contain energy at this frequency. Hence, it is shown that frequencies outside the input signal can be excited via the quadratic terms. In addition to this, it should be noted that an extra excitation at $\omega = 0$ can be observed too.

The erratic shape of the second order response graph results from the random phase that was adopted in the formulation of the input signal, see Equation (30). From this it follows that the amplitude of the second order response is input phase dependent.

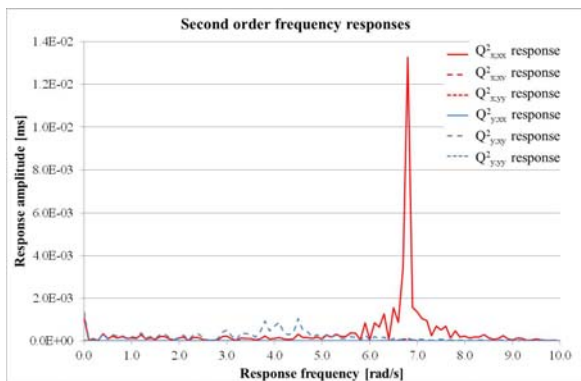


Figure 7. Second order frequency responses non-operating turbine blade.

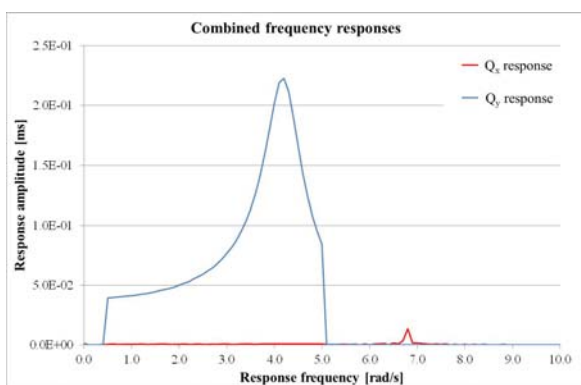


Figure 8. Combined frequency responses non-operating turbine blade.

Figure 8 depicts the combined first and second order responses. The total response is dominated by the response in y direction. The quadratic terms do not contribute much to this outcome. The peak response in x direction, that was observed in Figure 7 cannot completely be neglected. For a feathered blade it shows to be the main contribution in x direction.

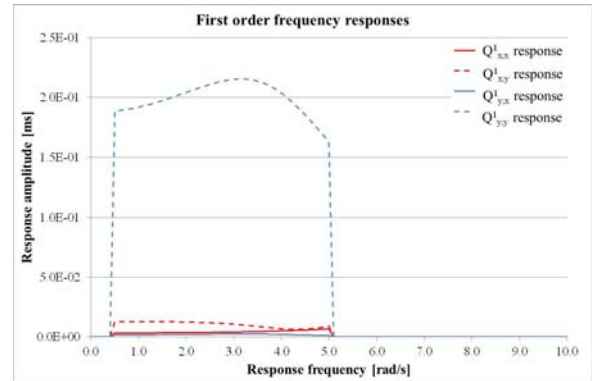


Figure 9. First order frequency responses operating turbine blade.

4.4 Operating turbine

In contrast to the non-operating turbine, the blade is now given a rotational speed of 12.1 rpm. This coincides with the rated rotor speed of the adopted turbine. The corresponding mean wind velocity is 11.4 m/s. Blade pitch is set at 0.1. All other parameters are the same as in the previous non-operating case. In addition it should be mentioned that the effect of rotation is not processed in excitation signal.

The first order response is dominated by the vibrations in y direction resulting from excitation in y direction (see Figure 9), which – due to the small pitch angle – can be referred to as flap wise motion. The shape of the response graph reveals the overdamped character of the motion, which was already referred to in section 4.1. The responses in edge wise direction are shown to be much smaller.

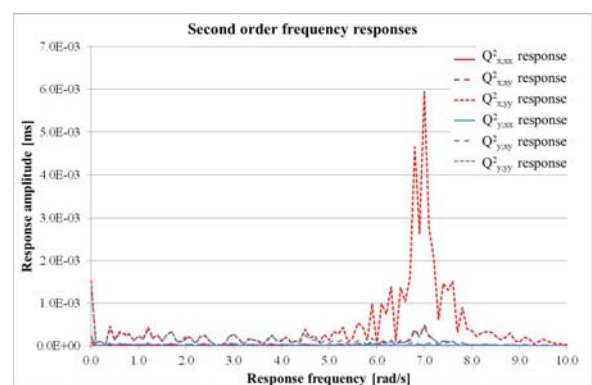


Figure 10. Second order frequency responses operating turbine blade.

The second order responses, see Figure 10, show content in x direction. The main response takes place at frequencies that are not present in the excitation signal. Nevertheless, the peak response, at the edge wise natural frequency, is still an order of magnitude smaller than the corresponding linear response. This can more clearly be seen in Figure 11, which shows the

combined responses. The second order results do not alter the first order response much.

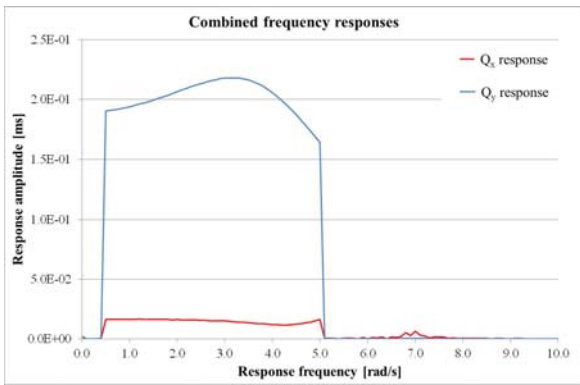


Figure 11. Combined frequency responses operating turbine blade.

4.5 Response without added damping

The combined linear and quadratic dynamic responses for a turbine blade of both a non-operating and an operating turbine have been determined. These total responses are now compared to the frequency responses while neglecting the added damping, see Figure 12 and Figure 13.

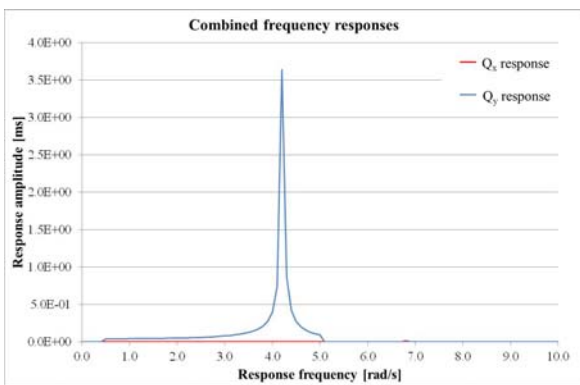


Figure 12. Combined frequency responses non-operating turbine blade without added damping.

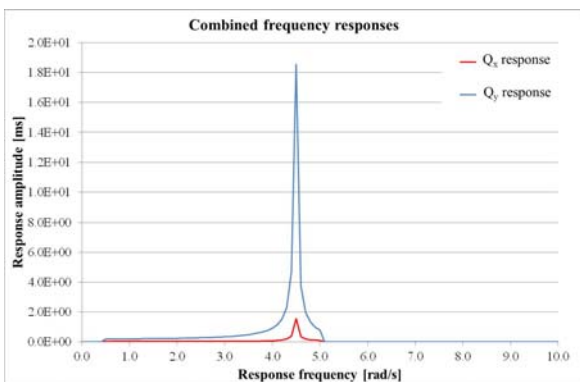


Figure 13. Combined frequency responses operating turbine blade without added damping.

When comparing Figure 12 to Figure 8, the strong damping of the response in y direction can immediately be recognized. The structural motion reduces the peak an order of magnitude. This effect is even stronger for the operating blade, where the

added damping decreases the flap wise response by two orders of magnitude. These results are related to the first order responses and confirm previous research results (for instance [16]).

Figure 14 and Figure 15 provide a more detailed view on the second order responses without added damping. When comparing these graphs to their damped equivalents, Figure 7 and Figure 10, a remarkable aspect can be distinguished. While the y contributions reduce due to the structural response, the added damping for the motion in x direction is negative, i.e., the peak values increase when added damping is accounted for. An explanation for this effect can be found in Equation (16). Acknowledging the dominance of the lift term, the second term of the equation, it follows that the contribution of the structural motion, which is negative for the linear case, gives a positive quadratic contribution to the forcing. This effect is observed for both the non-operating and the operating turbine.

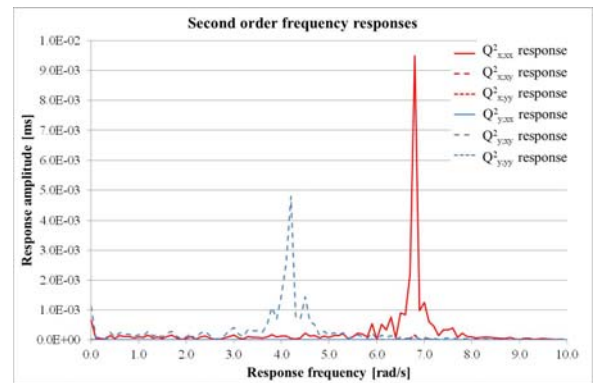


Figure 14. Second order frequency responses non-operating turbine blade without added damping.

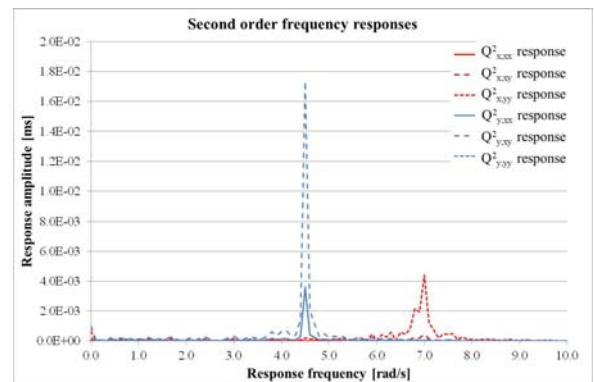


Figure 15. Second order frequency responses non-operating turbine blade without added damping.

5 CONCLUSIONS

This paper describes the derivation of a reduced 2DOF model for a wind turbine blade. The coupled nonlinear wind excitation, including structural motion was elaborated and the structural response was analyzed in the frequency domain. To this end, use was made of the Volterra series expansion. The estimation of the contribution of the quadratic forcing components was the main purpose of this work.

Dynamic responses were determined for both a non-operating blade and an operating blade. Use was made of the

blade characteristics of the NREL5 turbine. As excitation, additionally to the mean wind speed, a band-limited white noise signal was adopted, which acted simultaneously on both degrees of freedom.

The quadratic terms in the forcing equations did not show to contribute much to the total responses. Some second order responses were shown to be negatively damped due to the structural motion. As the higher order response is strongly input dependent, implying that no linear relation between input and output exists, the response to different input signals should still be investigated.

Unavoidably, the presented approach carries some limitations. First, the geometrically linear blade formulation does not allow for blade twist along the longitudinal axis. Its validity for larger deformations is limited too. Second, the modal reduction is restricted to the first modes only. Since the adopted modes are not adjusted for secondary effects as centrifugal stiffening and added damping, their validity may be poor. Torsional motion is not incorporated, implying that variations in angle of attack are not fully accounted for. Furthermore, the aeroelastic relations, which are functions of this angle of attack are assumed to be linear. These relations are only valid for attached flows, implying that the angle of attack should be relatively small. Last of all, due to the coupled flap and edge wise excitation, also cubic and even higher nonlinearities appear in the forcing formulation. These terms have been neglected.

ACKNOWLEDGMENTS

This work is supported by the Far and Large Offshore Wind (FLOW) innovation program.

REFERENCES

- [1] M.H. Hansen, M. Gaunaa, and H.A. Madsen. *A Beddoes-Leishman type dynamic stall model in state-space and indicial formulations*. Risø-R-1354(EN). Risø National Laboratory, Roskilde, Denmark, June 2004.
- [2] V.A. Riziotis, S.G. Voutsinas, E.S. Politis, and P.K. Chaviaropoulos. *Aeroelastic stability of wind turbines: the problem, the methods and the issues*. Wind Energy, 7: 373-392, 2004.
- [3] P.K. Chaviaropoulos. *Flap/lead-lag aeroelastic stability of wind turbine blades*. Wind Energy, 4:183-200, 2001.
- [4] W.J. Rugh. *Nonlinear system theory*. The John Hopkins University Press, Baltimore, Maryland, 1981.
- [5] C. Hayashi. *Nonlinear oscillations in physical systems*. McGraw-Hill, New York, NY, 1964.
- [6] K. Worden, G. Manson, and G.R. Tomlinson. *A harmonic probing algorithm for the multi-input Volterra series*. Journal of Sound and Vibration, 201(1): 67-84, 1997.
- [7] A. Kareem. *Nonlinear wind velocity term and response of compliant offshore structures*. Journal of Engineering Mechanics, 110: 1573-1578, 1984.
- [8] S. Benfratello, G. Falsone, and G. Muscolino. *Influence of the quadratic term in the alongwind stochastic response of SDOF structures*. Engineering Structures, 18(9): 685-695, 1996.
- [9] A. Kareem, M.A. Tognarelli, and K.R. Gurley. *Modeling and analysis of quadratic term in the wind effects on structures*. Journal of Wind Engineering and Industrial Aerodynamics, 74-76: 1101-1110, 1998.
- [10] S. Benfratello, M. Di Paola, and P.D. Spanos. *Stochastic response of MDOF wind-excited structures by means of Volterra series approach*. Journal of Wind Engineering and Industrial Aerodynamics, 74:1135-1145, 1998.
- [11] A. Kareem, J. Shao, and Tognarelli. *Surge response statistics of tension leg platforms under wind and wave loads: a statistical quadratization approach*. Probabilistic Engineering Mechanics, 10: 225-240, 1995.
- [12] L. Carassale and A. Kareem. *Modeling nonlinear systems by Volterra series*. Journal of Engineering Mechanics, 136: 801-818, 2010.
- [13] M. Balajewicz, F. Nitzsche, and D. Feszty. *Application of multi-input Volterra theory to nonlinear multi-degree-of-freedom aerodynamic systems*. AIAA Journal, 48(1): 56-62, 2010.
- [14] J. Jonkman, S. Butterfield, W. Musial, and Scott G. *Definition of a 5-MW reference wind turbine for offshore system development*. Technical Report NREL/TP-500-38060, National Renewable Energy Laboratory, Golden, Colorado, February 2009.
- [15] T. Burton, N. Jenkins, D. Sharpe, and E. Bossanyi. *Wind energy handbook*. Wiley, West Sussex, UK, second edition, 2011.
- [16] G. Bir and J. Jonkman. *Aeroelastic instabilities of large offshore and onshore wind turbines*. In Journal of Physics: Conference Series, volume 75. IOP Publishing, 2007.